Fuel 346 (2023) 128357

Contents lists available at ScienceDirect

Fuel

journal homepage: www.elsevier.com/locate/fuel

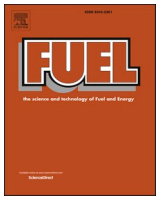

Full Length Article

A molecular investigation on the effects of OME_X addition on soot inception of diesel pyrolysis

Zhihao Xing, Mengwei Yu, Cheng Chen, Xi Jiang *

School of Engineering and Materials Science, Queen Mary University of London, Mile End Road, London E1 4NS, UK

ARTICLE INFO

Keywords:
Diesel
Oxymethylene dimethyl ethers
Pyrolysis
Reactive molecular dynamics
Soot

ABSTRACT

This study aimed at revealing the atomic-level chemical pathways involved in the soot inception inhibition of diesel pyrolysis with oxymethylene dimethyl ether (OME_X) addition. Using the reactive force field parameters in molecular dynamics simulation, the results effectively identified the specific pathways of OME_3 pyrolysis and soot inception, via the analysis of the conversion of three main species: CH_2O, $CH_3O^{\bullet}$, and $^{\bullet}CH_3$, generated from the initial decomposition of OME_3. It has been found that CH_2O molecule would be converted to CO through continuous dehydrogenation, and the carbon atoms convertered into CO would not participate in forming soot precursors, thus reducing soot formation. The oxidizing groups (mainly $^{\bullet}OH$) are primarily produced from the $CH_3O^{\bullet}$ radicals. These oxidizing species would react with small gaseous soot precursors to form stable oxides, thus inhibiting soot formation. However, this influence is relatively small under conditions where no oxygen is involved. The $^{\bullet}CH_3$ radicals would participate in the formation of soot precursors. In this study, it was observed that the addition of OME_3 did not reduce the number of main gaseous precursors of polycyclic aromatic hydrocarbons such as C_2H_2, $^{\bullet}C_2H_3$, and $^{\bullet}C_3H_3$ during diesel-OME_3 co-pyrolysis, because there were reactions between $^{\bullet}CH_3$ radicals and C_1 and C_2 species to form C_2 and C_3 hydrocarbon products. Based on the simulation results, the process from diesel decomposition to incipient soot production under the effects of OME_3 is panoramically demonstrated. It is also found that the chain length increase of OME_X with a fixed molar fraction does not influence soot inhibition noticeably. Increasing the proportion of OME_X added to diesel helps reduce soot as carbon atoms involved in the formation of soot precursors are reduced, and more oxidizing species would be produced to slow the formation of gaseous soot precursors.

1. Introduction

Although fossil fuels are gradually replaced by renewable energy sources such as wind, solar, and bioenergy, there are difficult-to-decarbonise applications such as sea, road freight and air transport. Due to the major challenges associated with decarbonisation, fossil fuels continue to play an essential part in the energy supply chain. Long-distance transport applications and heavey goods vehicles, such as marine and road freight transport, rely significantly on diesel combustion due to the high efficiency of the engine, high energy density and relatively low cost of the fuel. However, one of the biggest problems with burning diesel fuels is soot production, which has to be urgently reduced due to the environmental concerns.

Soot, also known as black carbon, is aggregated carbonaceous spherules with graphitic structures that are produced by the incomplete combustion of fossil fuels, biofuels, and biomass [1]. The mechanism of soot formation is generally understood. It is known that six commonly recognized processes are involved in the transformation of liquid or vapour hydrocarbons into solid soot particles, including fuel pyrolysis, nucleation, coalescence, surface growth, agglomeration, and oxidation [2]. However, owing to the complex process that involves gas-phase chemistry of primary fuel components, heterogeneous interactions on the surface of soot particles, and particle aerosol dynamics, detailed soot formation modelling remains challenging. Among the different stages in soot formation, particle nucleation, which is the shift from the gas-phase precursors to nascent condensed-phase particles, is probably the least understood area with numerous debates [3]. Soot has a major impact on climate change, with a significant global warming effect – possibly second only to CO_2 [4], and soot is toxic that harms human health [5]. Studying the mechanisms of carbon soot production is essential to find ways of suppressing its production. Any actions taken to reduce soot emissions can concurrently help human health protection and climate

* Corresponding author.
E-mail address: xi.jiang@qmul.ac.uk (X. Jiang).

https://doi.org/10.1016/j.fuel.2023.128357
Received 14 December 2022; Received in revised form 10 March 2023; Accepted 5 April 2023
Available online 14 April 2023

change mitigation.

It has been demonstrated that adding oxygenated biofuel effectively lowers soot emissions during diesel combustion in diesel engines [3]. The presence of oxygen atoms in oxygenated biofuel can immobilise some of the carbon atoms in the fuel and prevent them from forming polycyclic aromatic hydrocarbons (PAHs) [6], which are commonly known as the precursors for soot [7]. Due to their accessibility, ease of manufacturing, and favourable environmental effects, biodiesel and alcohols are among the oxygenated biofuel additions that have attracted the most attention [8]. However, the comparatively low oxygen content in biodiesel makes it less effective in mitagating soot production. Meanwhile, alcohols have a low Cetane number, delaying the ignition of the fuel [9]. The corrosiveness is also a big problem in the storage and engine applications of alcohol fuels [10].

Oxymethylene dimethyl ether (OME_X) is a class of dimethyl ether (DME) derivatives that can be produced from a range of waste feedstocks and biomass, thereby avoiding new fossil carbon from entering the supply chain. OME_X includes several oxymethylene (-O-CH_2-) groups in the molecule $H_3CO(CH_2O)_XCH_3$ with x (also represented by n in the literature) typically 1–8 where larger x corresponds to higher molecular mass and boiling points (x = 3–5 possess liquid properties similar to diesel), while DME CH_3OCH_3 (gaseous at ambient temperature and pressure) is equivalent to OME_0. As a clean alternative of diesel, a range of methodologies and processes have been used for the synthesis of OME_X. In addition, OME_X can be produced from renewable energy stored via catalytic conversion of hydrogen (H_2) and carbon dioxide (CO_2), as an electrofuel (or e-fuel), thereby used as a sustainable energy carrier. Nonetheless, the supply chain challenges including the high production costs of OME_X continue to be a barrier to its widespread use, as the production processes of $OME_{3\text{-}5}$ fuel may cost 1.5–3.6 times more than fossil-based diesel [11]. OME_X is considered to be a promising alternative oxygenated fuel due to its excellent physicochemical properties [12,13]. Unlike biodiesel and alcohols, OME_X have high oxygen content (nearly 50% by mass) and a high Cetane number [14], making it more suitable to be used as alternative oxygenated fuel than biodiesel and alcohols. However, OME_X has a relatively low calorific value compared with diesel [15]. Using OME_X alone as a fuel would result in increased fuel consumption, so blending OME_X with diesel as an additive is currently a promising strategy from both economic and emission suppression perspectives [16]. Experiments have shown that adding OME_X into diesel could increase combustion efficiency [9,17]. OME_X helps provide better oxidation conditions, leading to more thorough combustion than regular diesel fuel [18], and the high Cetane number ensures a high overall reaction rate [19]. The diesel-OME_X fuel mix can be used directly in existing diesel engines without structural adjustments [20,21]. Moreover, due to increased oxygen content and the absence of C-C bonds, the combustion of OME_X would produce less soot than diesel [22]. The experimental results of Popp et al. [23] show that even if only 20% of OME_X is added to the diesel, Particulate matter (PM) is reduced by more than 60%. Lin et al. [24] used a single-cylinder diesel engine to investigate the influence of the addition of OME_3 on PM emission. They suggested that OME_3 shows great potential in suppressing soot. Liu et al. [25] tested the combustion and emission characteristics of diesel/$OME_{3\text{-}4}$ blends in a light-duty diesel engine and found that the engine could function normally with blend fuel ratios containing less than 30% $OME_{3\text{-}4}$. Additionally, the inclusion of $OME_{3\text{-}4}$ in the blend resulted in a notable decrease in both soot and CO emissions.

The properties of OME_X vary with different chain lengths (value of x or n). For example, DME (or OME_0) is a gaseous fuel under normal conditions, making it difficult to be applied directly in diesel engines [9]. The molecular structure of dimethoxy methane (DMM) is CH_3O-CH_2OCH_3. It is a liquid fuel, but its Cetane number is very low (29) [9], which is far below the standard Cetane value of diesel (51) to ensure efficient diesel engine operation [26]. The higher molecular weight and lower vapour pressure make OME_X with $x \geq 2$ a more suitable additive than DME and DMM [20], but OME_2 has a low flash point, while the fuel melting points will be too high and the diesel-OME_X blended fuel will condense at low temperatures for $x \geq 5$ [21]. In general, the miscibility of diesel-OME_X blends decreases with the increasing chain length [27]. Thus, OME_3 and OME_4 are considered as ideal additives for diesel. Although adding more OME_X to diesel will introduce more oxygen atoms and thus inhibit soot production by trapping more carbon atoms, the fuel properties such as heating value and Cetane number would be influenced [28]. Meanwhile, small amounts of OME_X addition is not effective in inhibiting carbon soot production. Tan et al. [29] found that when OME_3 was blended with ethylene at 5%, the production of soot vulume fraction even increased due to the $^{\bullet}CH_3$ produced by OME_3. A 20% OME_X addition is usually considered as effective [30].

While OME_X has shown promising results as an oxygenated additive fuel that can inhibit soot production during diesel pyrolysis and combustion, further research is needed to understand the specific mechanisms by which OME_X exerts this effect. To study how OME_3 affects carbon particle production when blended with ethylene, Ferraro et al. [31] performed numerical simulations based on the method of conditional quadrature method of moments. They discovered that a further soot reduction might be promoted by a faster production of partially oxidized products in the gas-phase kinetics, and higher C═O functionalities were observed in their particle samples. The experimental results from Liu et al. [32] showed that OME_3 enhances the reactivity of soot oxidation, with the effect being more pronounced during the oxidation stage than the surface development stage. By utilizing high-speed spectroscopy, Pastor et al. [33] discovered that the chemiluminescence radiation from $^{\bullet}OH$ radicals is strong throughout the entire combustion process, and these radicals would break down the precursors responsible for forming soot. García-Oliver et al. [34] conducted computational fluid dynamics simulations and found that more OME_X added into the diesel would lead to lower equivalence ratios, speeding up the combustion process and making $^{\bullet}OH$ disappear sooner. Cai et al. [35] developed a reduced mechanism of OME_3-biodiesel. They found that the addition of OME_3 has no appreciable effects on the initial oxidation of biodiesel, whereas the species released during OME_3 combustion, such as $^{\bullet}OH$, CH_2O, and $^{\bullet}CH_3$, significantly aid in the oxidation of a precursor related to soot. These mechanisms were primarily based on several hypotheses drawn from logical experimental deductions and chemical intuitions, following the approach of macroscopic observations to microscopic mechanisms. There is still a lack of understanding on the specific pathways of OME_3 pyrolysis and soot inception to reveal the mechanism of soot inhibition by OME_X at the molecular level.

By examining the physical movements of atoms and molecules, molecular dynamics (MD) simulations can be used to develop more detailed soot inhibition mechanisms of OME_X. The basic idea of MD is to obtain thermodynamic and kinetic information about the system by solving Newton's equations of motion. The coordinates of each atom can be traced at different moments in time. The reactive force field (ReaxFF) based MD method has been widely used in the research of the mechanism of soot production [36–38]. The force field parameters are calculated from quantum mechanics (QM) and then extensively trained, making ReaxFF feasible for large-scale reactive systems, inheriting similar accuracy of QM but with substantially reduced computational expenses. In our previous study, the soot precursor mitigation potential of some typical oxygenated additives during the combustion of diesel-oxygenated addictives was tested by using ReaxFF [39]. The results show that the chemical structure of the oxygenated additive has a strong influence on the soot inhibition capacity.

In this study, we performed ReaxFF simulations to analyse how OME_X affects the soot inception in the diesel-OME_X blends. The OME_3 is chosen as a typical OME_X in the analysis of chemical mechanisms. The effects of chain length and the content of the OME_X are also quantified. Section 2 briefly presents the computational method. Section 3 presents detailed results from the analysis of the chemical pathways of the pyrolysis of OME_3, followed by a quantitative analysis of the effects of OME_3 on soot inception of diesel. Comparative results indicating the

effects of chain length of OME_X and the content of OME_3 on soot formation in diesel-OME_X systems are then presented. Based on the MD results, the reaction pathways of soot inception of diesel-OME_3 pyrolysis and how OME_3 affect the process are panoramically demonstrated. Finally, conclusions are drawn.

2. Computational methods

2.1. ReaxFF reactive force field

In molecular dynamics simulation, the force fields used can be divided into the classical and reactive force fields according to whether the formation of chemical bonds of atoms within a molecule can be simulated. ReaxFF force field uses a relationship between bond distance and bond order, and a relationship between bond order and bond energy, to allow for the formation, transition, and complete dissociation of chemical bonds between atoms. The ReaxFF force field was developed by van Duin et al. [40] to perform large-scale chemical system molecular dynamics simulations. It uses the following function for energy calculation:

$$E_{system} = E_{bond} + E_{over} + E_{under} + E_{val} + E_{pen} + E_{tors} + E_{conj} + E_{vdWaals} + E_{coulomb} \quad (1)$$

where E_{system} on the left-hand side of Eq. (1) represents the energy of the system, while the terms on the right-hand side of Eq. (1) represent the bond energy, the over- and under-coordination terms, the valence angle energy, the penalty energy, the torsion energy, the conjugation energy, the non-bond van der Waals and Coulomb interactions, respectively. There are mainly two sets of reactive force field parameters used in the MD simulations of hydrocarbon pyrolysis and combustion simulations, including CHO_{2008} [41] and CHO_{2016} [42]. The CHO_{2016} is the extension of CHO_{2008}, which makes up for the fact that CHO_{2008} can only predict larger hydrocarbons (>C_3) and allows the study of soot generation. Our previous study evaluated the feasibility of the two sets of parameters in predicting the incipient soot growing process [39] and found the improved CHO_{2016} parameters can predict the particle growth and the continuous dehydrogenation process during diesel combustion. The CHO_{2016} parameters are used in this study, as they are suitable for analysing the formation and consumption of soot precursors (C_2-C_3) and the pyrolysis products of OME_X like CH_2O, CH_3O•, and •CH_3, and accordingly that can better describe the soot generation process during the pyrolysis of diesel-OME_X blends.

2.2. Construction of the fuel model and simulation details

In practice, the components of diesel fuel are very complex and cannot be represented by a single chemical species. Although diesel is very rich in composition, it is primarily made up of the following chemical components: n-alkanes, isoalkanes, cycloalkanes and aromatics, with the carbon numbers of the different components ranging from C_{10} to C_{22} [43]. Considering the complexity and difficulty of investigating diesel-OME_X blends using experimental methods, numerical simulations using surrogate models offer an effective means to obtain fundamental understandings on the utilisation of the fuel blends. In this study, the diesel surrogate fuel model of Qian et al. [44] is employed in the MD simulation, which includes the typical chemical components in diesel and is capable of properly reproducing the combustion characteristics under the conditions of actual engine combustion. This surrogate model is constructed by 41.3% n-hexadecane (n-HXD, $C_{16}H_{34}$), 36.8% 2,2,4,4,6,8,8-heptamethylnonane (HMN, $C_{16}H_{34}$), and 21.9% 1-methylnaphthalene (1-MNT, $C_{11}H_{10}$). The molecular structures and chemical formulas of each diesel component and the general molecular formula of OME_X are shown in Fig. 1. The density of all the simulated systems was set to be 0.2 g/cm^3.

The detailed system constructions are shown in Table 1. As a baseline, System 1 is built with pure diesel surrogate molecules. Systems 2 to 6 are composed of diesel with different molar ratios of OME_3 added from 5% to 50%. The construction of different systems follows the same rule: the total carbon number in each system is approximately the same at around 2160, in order to quantify the effect of OME_X on soot inception and to study the number of carbon atoms in the incipient soot finally generated. To analyse the influence of the different structure (chain length) of the OME_X on soot inception, the molar fractions of different components in Systems 7 and 8 are consistent with System 4 (diesel with 20% OME_3 added). The only difference is that OME_1 and OME_5 are used in Systems 7 and 8, respectively.

All the simulations are performed using the open-source package Large-scale Atomic/Molecular Massively Parallel Simulator (LAMMPS) [45] with the latest developed CHO_{2016} ReaxFF force field. Periodic boundary conditions are employed in all three directions. Before simulations, each system was geometrically optimised using the Dreiding force field [46]. The optimised initial boxes of the pure diesel system and the system of diesel with 20% OME_3 added are shown in Fig. 2. Then reactive molecular dynamics simulations were performed with the isothermal-isochoric ensemble for 2 ns at 3000 K with a 0.25 fs timestep. In ReaxFF MD simulations, using relatively high temperature to speed up reactions is a common strategy, so that chemical reactions can take place in the very limited simulation time. This approach is believed to mainly affect reaction rates rather than reaction pathways. Zhao et al. [47] simulated the soot formation under the condition of 2560 K for an extended period of time and compared the results to those obtained at higher temperature, and they found that high temperatures (up to 3060 K) only speed up chemical reactions and do not significantly alter the soot-forming pathway. The flame temperature measurements from Tan et al. [29] suggested that the addition of the OME_3 has a negligible influence on the flame temperature profiles, and the differences in soot formation in flames are more likely related to chemical rather than temperature effects. In the MD simulation, chemical factors were the dominant influence, while certain physical factors such as the effect of pressure and turbulence during the combustion process were not considered. The species information was recorded every 100 fs. The atomic coordinates and bonding information were recorded every 250 fs. The Nosé-Hoover thermostat algorithm controls the system

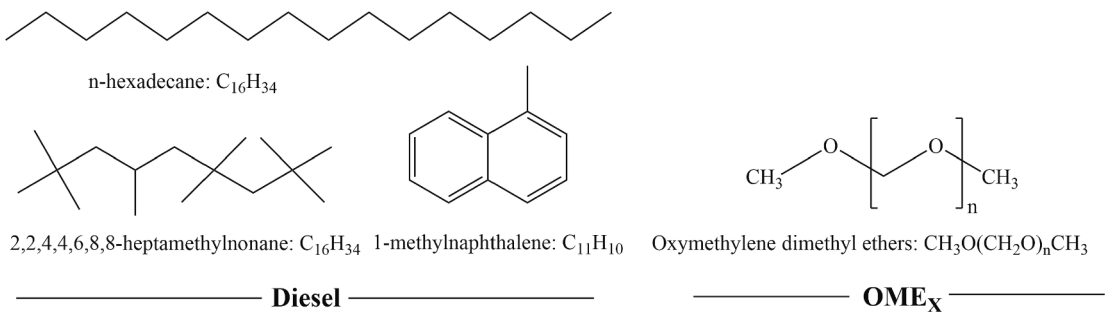

Fig. 1. The molecular structures and chemical formulas of diesel surrogate fuel and the OME_X.

Table 1
Detailed system constructions.

No. system	n-HXD molecules	HMN molecules	1-MNT molecules	OME_3 molecules	Number of C	Content
S1	60	53	32	0	2160	Pure Diesel
S2	59	52	31	8	2157	Diesel with 5% OME_3
S3	58	51	31	15	2160	Diesel with 10% OME_3
S4	55	49	29	35	2158	Diesel with 20% OME_3
S5	49	43	26	80	2158	Diesel with 40% OME_3
S6	45	40	24	107	2159	Diesel with 50% OME_3

No. system	n-HXD molecules	HMN molecules	1-MNT molecules	$OME_{1,5}$ molecules	Content
S7	55	49	29	35	Diesel with OME_1
S8	55	49	29	35	Diesel with OME_5

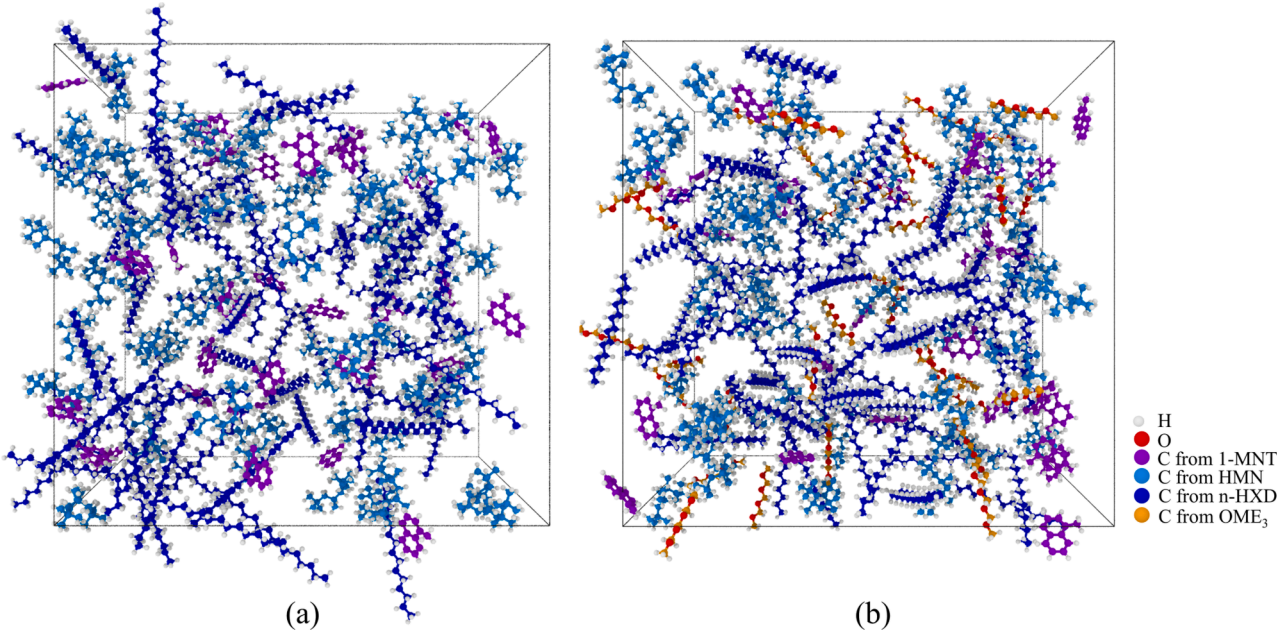

Fig. 2. Systems of (a) pure diesel and (b) diesel with 20% OME_3 added.

temperature with a damping constant of 25 fs (100 timesteps). The bond-order cutoff is set to be 0.3, which had been tested to be an appropriate value in the simulations of pyrolysis and oxidation of hydrocarbon systems in previous studies [48,49]. To reduce calculation errors and to ensure that the simulation is statistically accurate, each case is averaged five times with different initial velocities and distribution of atomic coordinates. The simulation results were visualised by using OVITO Pro [50]. The reaction pathways were extracted from the atomic coordinates and bonding information using the ReacNetGenerator package developed by Zeng et al. [51].

3. Results and discussion

3.1. Pyrolysis of OME_3

To analyse the detailed reaction mechanisms of OME_3 pyrolysis, 40 OME_3 molecules (which were tested to be sufficient in the MD simulation) were put into a cubic simulation box with a density of 0.2 g/cm^3. The simulation lasts for 250 ps at a constant temperature of 3000 K. The initial pyrolysis pathways of OME_3 are shown in Fig. 3a. The unique structure of OME_3, not containing C-C bonds, is symmetric about the central carbon atom with the C-O and C-H bonds to the left and right, mirrored across the central carbon. The cleavage reaction of OME_3 begins with C-O bond breaking in four different locations, and the C-H bonds do not break in this process. This is due to the bond dissociation energy of the C-H bonds being higher than the C-O bond, especially the secondary C-H bonds, which are higher than those of the primary C-H bonds [52]. The percentage of bond breaking occurrence at the four locations showed that bond 4 broke with the highest percentage at 40.97%; this value was 34.15%, 12.68% and 12.2% for bonds 3, 2 and 1, respectively. This means that the closer to the middle the C-O bond is, the more fragile it is, which makes it more likely to break. For bonds 1 and 2, the chances of initial breaking are almost the same. For one OME_3 molecule, regardless of where bond breaking starts with, the end products are one $CH_3O^{\bullet}$ radical, one $^{\bullet}CH_3$ radical and three CH_2O molecules, which is in accordance with the general formula for the decomposition of OME_X, shown in $OME_X \rightarrow CH_3O^{\bullet} + {}^{\bullet}CH_3 + XCH_2O$ [53]. These initial reaction pathways are in good agreement with the simulation results of Wang et al. [48] and experimental inferences of Tan et al. [53].

In Fig. 3a, formaldehyde (CH_2O) molecules are removed from larger radicals (carbon number greater than 1) through C-O bond dissociation or β-scission reactions to form smaller radicals. CH_2O is the predominant product of the initial pyrolysis of OME_3. The detailed follow-up reactions of the main species (CH_2O, $CH_3O^{\bullet}$, $^{\bullet}CH_3$, and $^{\bullet}H$) produced by OME_3 pyrolysis are establishd in this study, as shown in Fig. 3b. The $CH_3O^{\bullet}$ radicals also produce CH_2O by dehydrogenation.

Fig. 4 shows the main consumption and production pathways of CH_2O during OME_3 pyrolysis. From Fig. 4, it can be seen that the dominant consumption pathway (48.27%) of CH_2O is $CH_2O \rightarrow {}^{\bullet}H + {}^{\bullet}CHO$. Some $^{\bullet}CHO$ would be produced from the hydrogen transfer

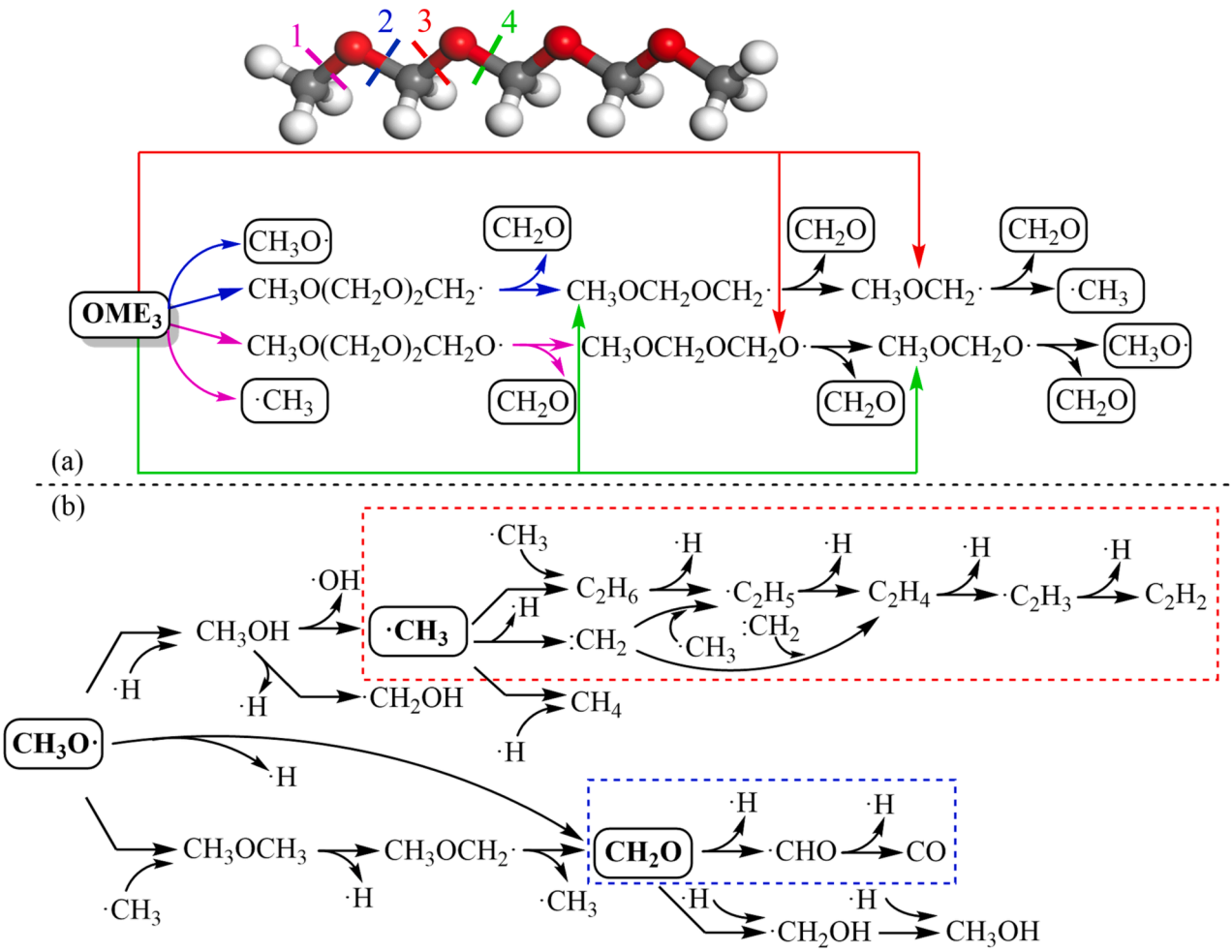

Fig. 3. (a) The initial reaction pathways of OME_3 pyrolysis; (b) detailed follow-up reactions of the primary species, where the ball-and-stick model represents the structure of OME_3.

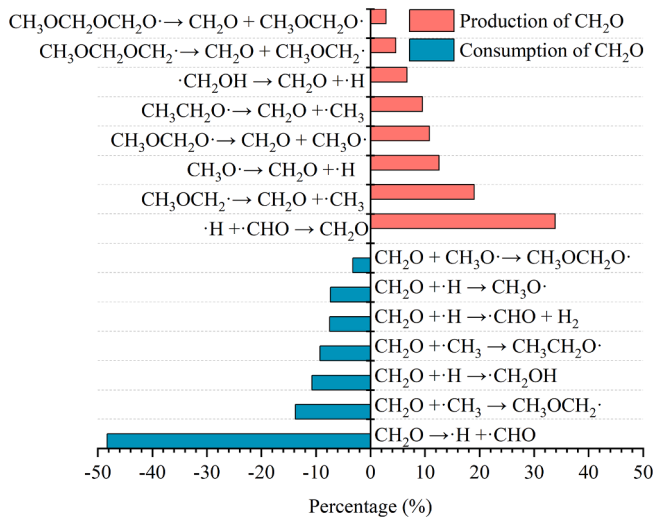

Fig. 4. Main consumption and production pathways of CH_2O during OME_3 pyrolysis.

reaction $CH_2O + •H \rightarrow •CHO + H_2$. The generated •CHO would then be converted into CO, preventing the carbon atoms from contributing to the generation of soot precursors [54]. This is the main reason for the soot inhibition in the co-pyrolysis of diesel and OME_3, which is outlined with the blue dashed line in Fig. 3b. It needs to be noticed that $•CH_2OH$ would be produced through the reaction $CH_2O + •H \rightarrow •CH_2OH$. Both the •CHO and $•CH_2OH$ are oxidizing groups, which would oxidize soot precursors to form stable oxides, thus slowing down the formation of the first benzene ring. However, this effect is quite small as both •CHO and $•CH_2OH$ radicals are unstable in high temprature. They will quickly be converted into CO and CH_2O, respectively. The reaction $•H + •CHO \rightarrow CH_2O$ is found to be the main production pathway of CH_2O, and this is a reversible reaction in which CH_2O is dehydrogenated to produce •CHO. In addition to the dehydrogenation of $CH_3O•$, CH_2O is mainly produced via the reactions $CH_3OCH_2• \rightarrow CH_2O + •CH_3$ and $CH_3OCH_2O• \rightarrow CH_2O + CH_3O•$. The former reaction occurs more frequently than the latter, because $CH_3OCH_2•$ would also be formed through the reaction $CH_3O• + •CH_3 \rightarrow CH_3OCH_3$ and CH_3OCH_3 would further form $CH_3OCH_2•$ through dehydrogenation.

Fig. 5 shows that main consumption and production pathways of $CH_3O•$ during OME_3 pyrolysis. From Fig. 5, it can be seen that the methoxy radicals ($CH_3O•$) are mainly produced by the decomposition of $CH_3OCH_2O•$ (37.37%), CH_3OCH_3 (26.39%) and OME_3 (17.43%). The dominant consumption pathway (46.39%) of $CH_3O•$ is to form CH_2O through dehydrogenation (46.39%), followed by the reaction $CH_3O• + •CH_3 \rightarrow CH_3OCH_3$ (29.16%). Compared with CH_2O, $CH_3O•$ has a higher reactivity. The $CH_3O•$ is an oxidizing group, which can react with other small hydrocarbons to form ethers. It can also form CH_3OH by adding a •H (4.7%). The CH_3OH can be converted to •OH, which would help suppress the formation of soot precursors. This effect is insignificant because no oxygen is involved in the pyrolysis simulations. It is reported

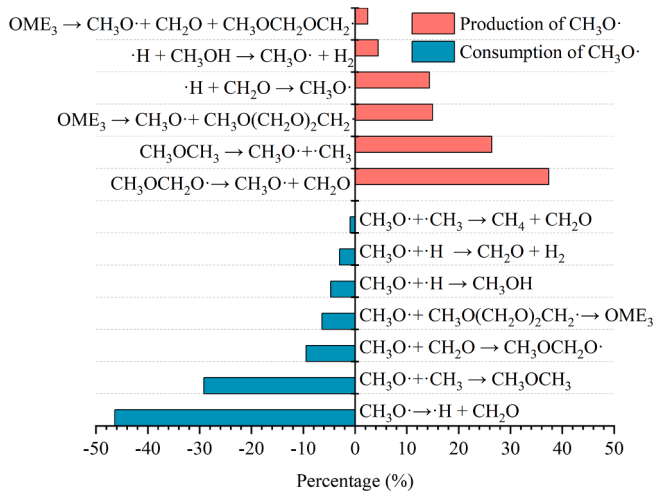

Fig. 5. Main consumption and production pathways of CH_3O• during OME_3 pyrolysis.

that under combustion conditions, the CH_3O• would produce more oxidizing species such as •O and HOO• through thermal dissociation or reaction with oxygen [32,53,55].

Unlike oxygen-containing groups CH_2O and CH_3O•, the methyl (•CH_3) would participate in the formation of PAHs. In Fig. 3b, the red dashed line outlines the detailed reaction pathways of soot precursor formation during OME_3 pyrolysis. The •CH_3 radical would produce the :CH_2 radical through dehydrogenation. The •CH_3 radical would also react with other •CH_3 radicals and :CH_2 radicals to form C_2H_6 and •C_2H_5, and then a variety of unsaturated C_2 species, such as •C_2H_3 and C_2H_2 would be produced by continuous dehydrogenation. •C_2H_3 and C_2H_2 are considered as the most critical species during soot formation [56] as they are the main reactive molecules that form the initial rings. In the H-abstraction-C_2H_2-addition (HACA) mechanism, C_2H_2 will be added to the active site on the aromatic molecule formed by the abstraction of a gaseous hydrogen atom [7]. However, this $C_1 \rightarrow C_2$ mechanism hardly occurred during the OME_3 pyrolysis. It can be seen from Fig. 6 that only a few •CH_3 would react with other small hydrocarbon species. The reaction pathway of •CH_3 is still mainly related to the initial pyrolysis of OME_3. The •CH_3 would primarily be consumed by reacting with oxygen-containing radicals, such as •OH (17.92%), CH_2O (25.92%), and CH_3O• (13.4%). It would also form methane (CH_4) by adding a •H (11.44%). The probability of the $C_1 \rightarrow C_2$ mechanism occurrence is significantly reduced, which could explain the near absence of soot production while burning pure OME_3. The main production pathway of •CH_3 is through the decomposition of CH_3OCH_2• (23.04%), CH_3OH (14.85%), CH_3CH_2O• (12.43%), and CH_3OCH_3 (12.11%). It is also noticable that •H is the most active strong oxidizing radical produced during the pyrolysis of OME_3. It was found that about 160 kinds of reactions were associated with •H during the simualtion, where there is about 100 kinds of reactions for •CH_3, and about 60 for CH_3O•. A significant volume of H_2 would be

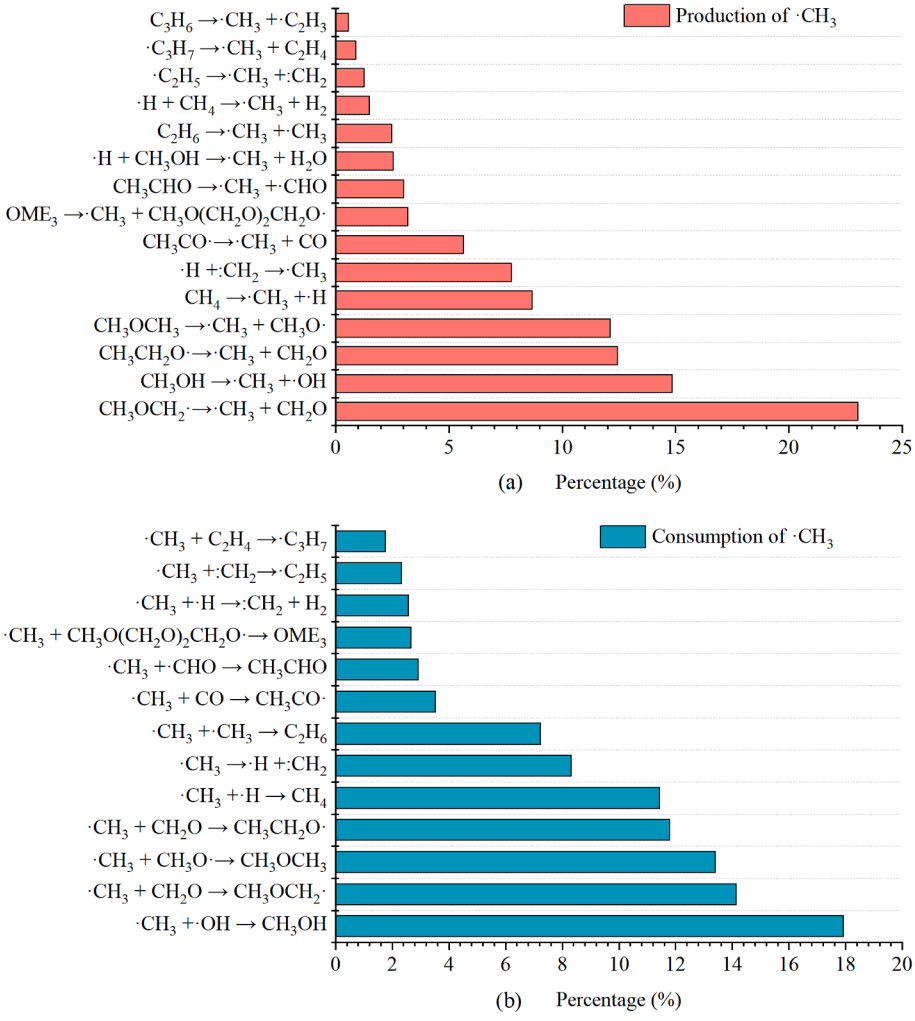

Fig. 6. Main reaction pathways of •CH_3 during OME_3 pyrolysis: (a) production; (b) consumption.

produced by the frequent collision of •H radicals.

3.2. The effects of OME_3 on soot inception of diesel

Fig. 7 shows the structures and chemical formulas of the largest incipient soot in diesel and diesel-OME_3 blends after 2 ns simulations. The addition of OME_3 reduces the size of the final generated incipient soot. In the diesel-OME_3 blends, the reactions begin with decomposition of the components in the mixture. It is found that HMN completed the initial cleverage in just 10.5 ps, while this value is 17.5 ps and 20.5 ps for OME_3 and n-HXD, respectively. Due to the stability of the aromatic ring, the 1-MNT spent 154.5 ps to complete pyrolysis. From the simulation results of Wang et al. [48], in the early stages of pyrolysis, OME_3 breaks down rapidly into small oxidizing radicals, creating a rich pool of free radicals and providing a suitable environment to promote the pyrolysis of diesel.

The classification of chemical species with regard to different carbon numbers used by Zheng et al. [57] and Wang et al. [38] is adopted in ths study. The $C_{1\text{-}4}$ fragments are considered gaseous soot precursors, which include the pyrolysis products of OME_X and oxidation products like CH_3OH, C_2H_4OH, and C_2H_3OH. Species of carbon numbers above 40 are thought to be incipient soot. The $C_{5\text{-}20}$ compounds are different diesel components and OME_3, which mainly include small PAH-like soot precursors and short carbon chains. The $C_{20\text{-}40}$ species are large PAH-like soot precursors and long unsaturated carbon chains which will become incipient soot. Fig. 8a shows the change in the proportion of different carbon-containing species in the system over time. The reactions start with a rapid decomposition of the various components of the diesel-OME_3 blends, accompanied by a rapid increase in C_1-C_4 species. The $C_{1\text{-}4}$ species reached a local maximum value at around 52 ps, which accounts for 75.19% of total products, while at the same time, the percentage of $C_{5\text{-}20}$ products reached a local minimum value of around 23.73%. Only a few (1.08%) $C_{20\text{-}40}$ species were produced. These products are formed mainly from the branched chains produced by 1-MNT after the completion of its first ring opening, combined with fragments from hydrocarbon cleavage. At this time, there is no $C_{\geq 40}$ species observed. Then $C_{1\text{-}4}$ species percentage decreased quickly, and their involvement in the formation of unsaturated long carbon chains as well as PAH-like soot precursors resulted in a gradual rise in $C_{5\text{-}20}$ and $C_{20\text{-}40}$ species. $C_{\geq 40}$ species start to emerge at around 200 ps. $C_{5\text{-}20}$ and $C_{20\text{-}40}$ species begin to decrease at 500 and 750 ps, respectively, and they, like $C_{1\text{-}4}$ species, are involved in the formation of incipient soot, causing a sustained increase in $C_{\geq 40}$ species. The proportion of species at each carbon number remains stable after 1750 ps, when the system is largely in balance.

The main oxygen-containing products are shown in Fig. 8b. The number of CH_2O molecules peaks at 111 at 23.1 ps. There are 35 OME_3 molecules in this system, and the amount of CH_2O is around three times that of OME_3, which is consistent with previous analysis of the OME_3 pyrolysis reaction pathway. CH_2O peaks only slightly later than the time of complete pyrolysis of OME_3 (17.5 ps), which means OME_3 breaks down quickly into small C_1 fragments at high temperature. The number of CH_3O• molecules peaks at 19 at 5.5 ps. Then due to its high reactivity, CH_3O• radicals are quickly consumed to form other species like CH_2O, causing the number of peak CH_2O molecules to be slightly more than three times the number of OME_3. The C═O double bond in CH_2O is very stable and difficult to break even at high temperature. The CO molecules are produced by the continuous dehydrogenation of CH_2O, which results in an increasing trend of CO molecules that is highly consistent with the decreasing trend of CH_2O molecules. The carbon fixed by oxygen to form CO will not participate in the formation of soot precursors. The number of CO molecules increased sharply before 750 ps, then its rate of increase began to slow down, and the number of molecules remained stable at 127. The •CHO radicals always exist in the system in tiny quantities because it can easily decompose to CO and combine with other small molecule products to form aldehydes. The H_2O molecules are mainly produced through the reactions: $•H + •OH \rightarrow H_2O$, $H_2 + •OH \rightarrow H_2O + •H$. The •OH is mainly produced from the decomposition reaction of methanol (CH_3OH).

Fig. 8c shows types of oxygen-containing products and the number of molecules containing oxygen atoms. The consumption and production of the main reactive oxygenated radicals (•CHO and •OH) during diesel-OME_3 blends pyrolysis are shown in Fig. 9 and Fig. 10, respectively. The number of molecules containing oxygen atoms increased sharply to 140 at 18.8 ps, which was only slightly later than the initial cleverage of OME_3. Then this value remained almost stable at 140, which is equal to the total oxygen number. This means oxygen-containing products contain essentially only one oxygen atom. The number of species of oxygen-containing products increased sharply, peaking at around 18 at 35.5 ps, then began to diminish. At the beginning of the pyrolysis, various reactive oxygenated products exist in the system, including mainly •OH, CH_3O•, •CHO. They are the products of complete pyrolysis of OME_3. The •CHO radicals are primarily produced by the decomposition (54.4%) and hydrogen transfer (15.2%) of CH_2O. The •CHO radicals would mostly be consumed by reaction $•CHO \rightarrow CO + •H$ (63.31%). This reaction occurred very fast, which caused only a few (1.4%) •CHO combining with small hydrocarbon radicals ($•CH_3$) to form aldehyde compound. Except for •CHO, the formation of other reactive oxygenated products are highly relevant to CH_3O•. At the beginning of the pyrolysis (0–35.5 ps), the system contains relatively high levels of $•CH_3O$. The most critical reactive oxygenated radicals •OH would be produced through the reaction: $CH_3O• + •H \rightarrow CH_3OH \rightarrow •CH_3 + •OH$. The C_1-C_2 species ($•CH_3$, C_2H_4,$•C_2H_3$ etc.) resulting from the complete pyrolysis of alkanes will combine with the •OH, and a few $•CH_2OH$ radicals would be

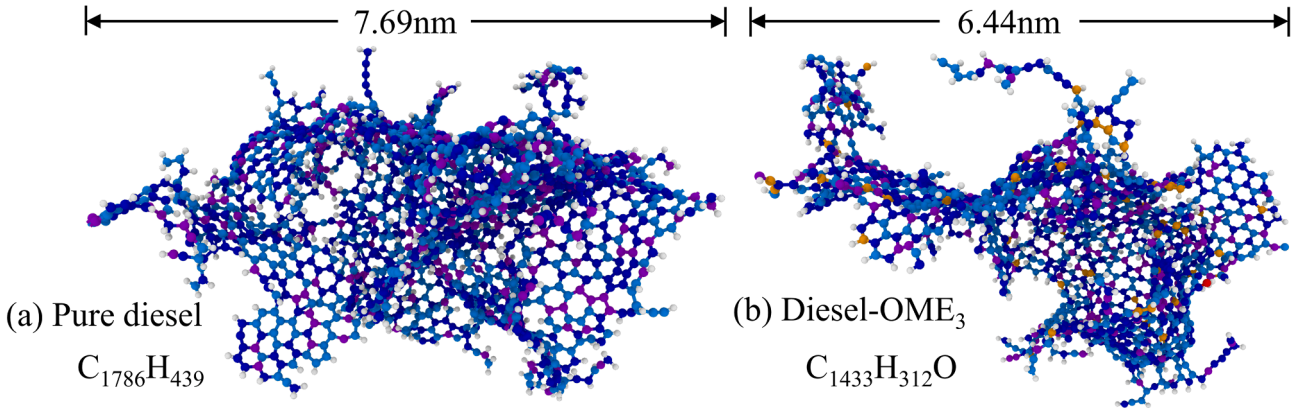

Fig. 7. The structures and chemical formulas of the largest incipient soot at 2 ns: (a) pure diesel; (b) diesel-OME_3 blends.

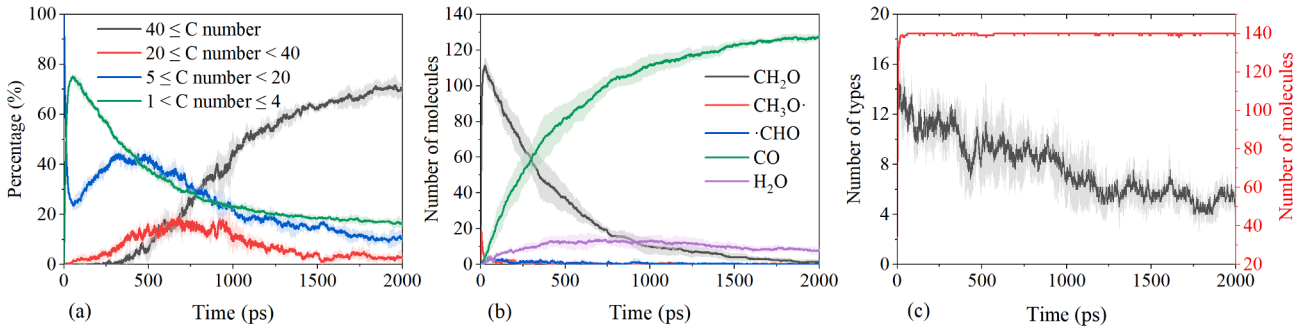

Fig. 8. (a) Percentage of different ranges of C number in the diesel-OME_3 system; (b) the main oxygen-containing products; (c) different types of oxygen-containing products (black line) and the number of molecules containing O atom (red line). (For interpretation of the references to colour in this figure legend, the reader is referred to the web version of this article.)

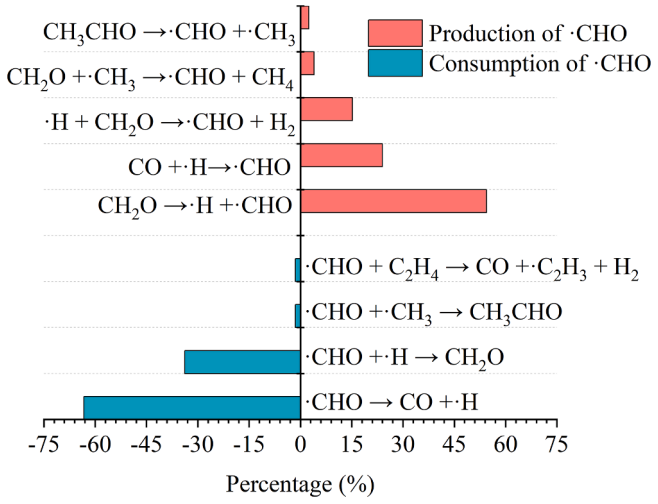

Fig. 9. Main consumption and production pathways of •CHO during Diesel-OME_3 pyrolysis.

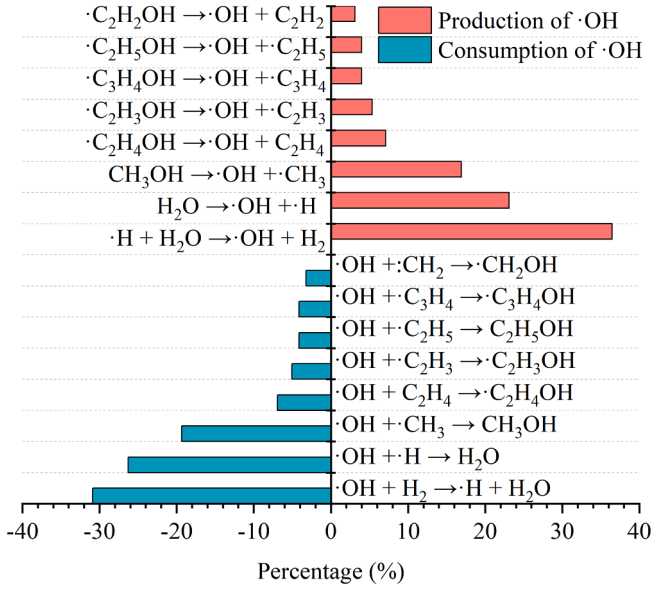

Fig. 10. Main consumption and production pathways of •OH during Diesel-OME_3 pyrolysis.

produced through the dehydrogenation of CH_3OH, which results in the occurrence of many different types of alcohol products such as CH_3OH, C_2H_4OH, C_2H_3OH, and C_2H_5OH. Then the types of oxygenated products begin to decrease due to the consumption of the CH_3O• and the consumption of •OH to form H_2O. The number of different types of oxygen-containing products does not change appreciably from 120 to 350 ps. Then there is a sharp decrease from 350 to 450 ps. It can be deduced that at this stage, more and more small molecules ($C_{1\text{-}4}$) combine quickly to form larger molecules, resulting in low concentrations of unsaturated gaseous molecules. The probability of collision between reactive oxygenated products and unsaturated gaseous species is reduced. The curve continued to fall until 1850 ps, and some •OH radicals were formed through the decomposition and hydrogen transfer of H_2O, causing some alcohol molecules to be produced. On the whole, the reactive oxygen-containing radicals play a significant role in the oxidation of the gaseous soot precursors of $C_{1\text{-}2}$ species, which occurs before the first benzene ring is formed. Only a tiny amount of •OH generated by the decomposition of H_2O will react with the PAHs during the continued growth phase of the benzene ring.

To further investigate the sources of carbon and oxygen atoms in the final produced CO, we have divided the sources of oxygen atoms into two categories: oxygen atoms at the end edge of the OME_3 are called O_e, and the oxygen atoms in the middle are called O_m. The source of carbon atoms is divided into three categories: C_d represents carbon atoms from diesel, C_e represents the carbon atoms from the end edge of the OME_3, and C_m represents the three carbon atoms in the middle of the OME_3.

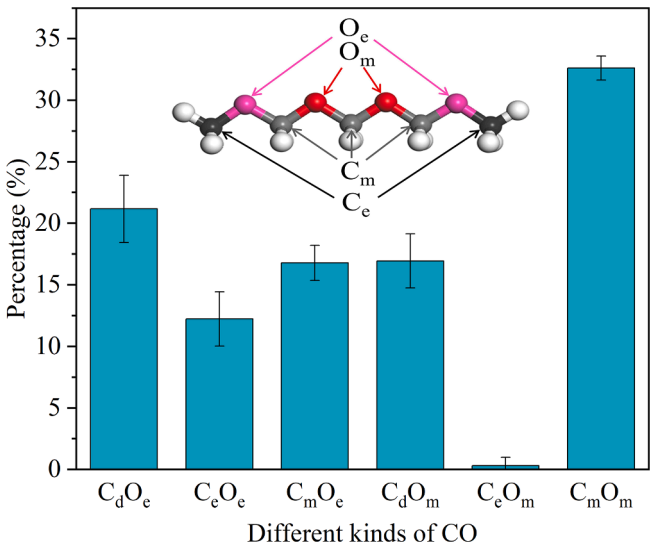

Fig. 11. Percentage of different CO in diesel-OME_3 systems at the end of the simulations, C_d represents carbon atoms from diesel.

Fig. 11 shows the percentage of different CO in diesel-OME_3 systems at the end of the simulations. The primary type of CO is C_mO_m (32.6%), even more than the sum of C_eO_e (12.22%), C_mO_e (16.77%), and C_eO_m (0.31%), which means the final CO is mainly produced by the carbon and oxygen atoms in the middle of OME_3. This is consistent with our analysis of the reaction pathway of OME_3. The C and O in the middle of the OME_3 are mainly released as $C_mH_2O_m$, and then C_mO_m is produced by the route $C_mH_2O_m \rightarrow {}^{\bullet}C_mHO_m \rightarrow C_mO_m$. C_dO_e has a more significant proportion than C_dO_m, which means O_e is more likely to react with carbon atoms in diesel compared to O_m. This is because, during the initial pyrolysis of OME_3, some O_e would be released in the form of $C_eH_3O_e{}^{\bullet}$, whereas the O_m is released only in the form of $C_mH_2O_m$. The chemical form in which the oxygen in OME_3 is combined with the carbon in diesel is further analysed. For C_dO_e, the first combination of O_e with C_d takes the form of CH_2O (48%), $^{\bullet}OH$ (44%), CO (4%), and $CH_3O^{\bullet}$ (4%), combined with carbon atoms containing the active site. For C_dO_m, the first combination of O_e with C_d takes the form of CH_2O (65.22%), $^{\bullet}OH$ (17.39%), and CO (17.39%). Compared to CH_2O molecules, $CH_3O^{\bullet}$ radicals have a higher reactivity. They can directly react with other hydrocarbon compounds or produce $^{\bullet}OH$ to oxidize hydrocarbon compounds. The typical reaction pathways of $^{\bullet}OH$ radical oxidizing hydrocarbon species to form CO are shown in Fig. 12. After connecting to the active site on the hydrocarbon species, the O-H bond in the $^{\bullet}OH$ radical would firstly break, then aldehydes species are produced and finally converted to CO. CO is hardly ever present in the form of C_eO_m, which means carbon atoms at the edge of the OME_3 can scarcely react with the middle oxygen atoms. On one hand, this is due to the relatively stable C═O double bond of CH_2O produced by C and O located in the middle of OME_3, making them hardly react with other species. On the other hand, the C_e is released in the form of $C_eH_3O_e{}^{\bullet}$ or $^{\bullet}C_eH_3$. The CO would be produced through the reaction $C_eH_3O_e{}^{\bullet} \rightarrow C_eH_2O_e \rightarrow {}^{\bullet}C_eHO_e \rightarrow C_eO_e$. The $^{\bullet}C_eH_3$ will participate in the formation of soot precursors.

Fig. 13 illustrates a panoramic view of the process, from initial diesel pyrolysis to soot inception, indicating how OME_3 influences this process. In Fig. 13, the atom tagging method is used to trace the carbon transformations during the formation of incipient soot, i.e., different colours are used to represent carbon atoms originating from different fuel components. The simulation results indicate that the initial reactions of the normal paraffin n-HXD are the same as the branched paraffin HMN, both involving a series of unimolecular C–C bond scissions and H-abstract reactions to generate smaller alkyl radicals. The main difference is that HMN tends to produce larger alkenes, such as linear alkene of propene and branched alkene of 2-methylpropene, due to its highly branched quaternary carbon structures [58]. During this process, a large amount of C_1 (mainly $^{\bullet}CH_3$) and C_2 (mainly $^{\bullet}C_2H_4$) species are released. As discussed previously, the reactive oxygen-containing groups produced by OME_3 would react with these C_1 and C_2 species to form stable oxides such as aldehydes, alcohols, and ethers, which inhibit the growth of incipient soot. The structures of typical oxides are shown in the central area of Fig. 13. The resonance-stabilized radicals (RSRs), e.g. propargyl ($^{\bullet}C_3H_3$) and cyclopentadienyl ($^{\bullet}C_5H_5$), would also be produced in this process. C_3H_3 is known as the key precursor in benzene formation via the reaction $^{\bullet}C_3H_3 + {}^{\bullet}C_3H_3 \rightarrow C_6H_6$. In recent years, it was also recognised as the initiator in the CHRCR (Clustering of Hydrocarbons by Radical Chain Reactions) model for radical chain reaction via the reaction $^{\bullet}C_3H_3 + C_2H_2 \rightarrow {}^{\bullet}C_5H_5$ [59]. As indicated by the precursors shown in Fig. 13, the simulation reveals the presence of cyclopentadienyl, which consists of $^{\bullet}C_3H_3$ generated by n-HXD and C_2H_2 produced by HMN.

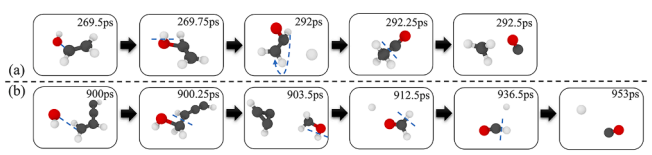

Fig. 12. Snapshots of $^{\bullet}OH$ radicals oxidizing hydrocarbon species to form carbon monoxides: (a) C-C bond breakage after hydrogen transfer of alcohol molecule; (b) $^{\bullet}OH$ radical promotes the oxidation of soot precursor to produce CH_2O molecule and eventually CO, where C, H and O atoms are represented in grey, white and red, respectively. (For interpretation of the references to colour in this figure legend, the reader is referred to the web version of this article.)

The aromatic ring structure of 1-MNT makes it more stable than n-HXD and HMN. The double ring structure of 1-MNT can be observed until 337 ps. Then the benzene rings of 1-MNT will break through the ring-opening reaction while the other ring remains intact. Immediately afterwards, another ring will open, and the structure with a long unsaturated chain connected to a slightly shorter unsaturated chain will be formed. Atom labelling indicated that the product is obtained from the initial pyrolysis of 1-MNT, rather than the recombination of other small molecule precursors. These unsaturated long-branched structures provide active sites for the attachment of other unsaturated $C_{1\text{-}3}$ hydrocarbons such as $^{\bullet}CH_3$, $^{\bullet}C_2H_3$, C_2H_2, and $^{\bullet}C_3H_3$, which would promote the formation of soot. Also, the oxidizing species (mainly $^{\bullet}OH$, together with $CH_3O^{\bullet}$, $^{\bullet}CHO$, and $^{\bullet}CH_2OH$) produced by OME_3 could occupy the active sites on long unsaturated carbon chains, thereby inhibiting further chain elongation. In addition to combining small hydrocarbons with the unsaturated carbon chains formed by 1-MNT, these small hydrocarbons also assemble themselves into unsaturated long carbon chains. It needs to be noticed that the $^{\bullet}CH_3$ produced by the breakage of the C-O bond of the edge of OME_3 would also participate in this process and promote the extension of the chains. These unsaturated long carbon chains then undergo cyclization and internal bridging to generate polycyclic aromatic hydrocarbons, which further combine through the side chain and internal bond cross-linking to form the incipient soot [60]. OME_3 is hardly involved in soot inception from the long unsaturated chains. Only small C_1-C_2 hydrocarbons such as $^{\bullet}CH_3$ and C_2H_2 produced by the OME_3 were found to be connected to the active sites. The $^{\bullet}OH$ produced by the decomposition of H_2O was occasionally found in the PAH-like molecules. Oxygen fixation of carbon to form CO is the most important reason for OME_3 to suppress soot formation during diesel pyrolysis. About 63% of the final CO is composed of C and O in the OME_3.

Fig. 14 displays the contributions of different carbon atoms in OME_3 to incipient soot. C_1 and C_5 represent the carbon atoms at the edge of the OME_3. They are actually the same kind of carbon atoms because of the symmetry of the OME_3 molecular structure and they contribute significantly to the production of incipient soot (58.88%). C_2 and C_4 are the adjacent carbon atoms to the C_1 and C_5. It is interesting to notice that the C_3, the carbon atom in the centre of OME_3, makes a slightly larger contribution (15.19%) to incipient soot than half of the sum of C_2 and C_4 (25.93%). This is because the initial cleavage OME_3 is more likely to break the C-O bond 4 shown in Fig. 3, which makes C_3 more exposed with increased probability of connecting to hydrocarbons.

As discussed previously, the effect of OME_3 on soot inception is mainly in the oxidation of the gaseous soot precursors. Here, we focus on the time evolutions of typical C_1-C_3 intermediates in pure diesel and diesel-OME_3 blends, as shown in Fig. 15. Compared with pure diesel system, more $^{\bullet}CH_3$ would be produced in the diesel-OME_3 system, as previously discussed, which are produced by the cleavage of C-O bond (bond 1 in Fig. 3) at the edge of the OME_3. The number of molecules of C_2H_4 produced in the pure diesel and diesel-OME_3 blends peaks at the same time (75 ps). They are mainly the pyrolysis products of the linear and branched alkanes. However, the maximum number of C_2H_4 molecules in the pure diesel system is higher than that in the diesel-OME_3 blends. This is due to the addition of OME_3, which reduces the number of diesel molecules in the mixture. The reduction of C_2H_4 molecules in the diesel-OME_3 system is significantly slower than in the pure diesel system. We analysed the frequency of main consumption pathways of $^{\bullet}CH_3$ from 75 to 220 ps. During this time frame, the amount of C_2H_4 molecules in the pure diesel system is greater, but the rate of consumption is slower than in the OME system. In the diesel-OME_3 system, there are many unsaturated C_1-C_3 hydrocarbon species produced by the pyrolysis of

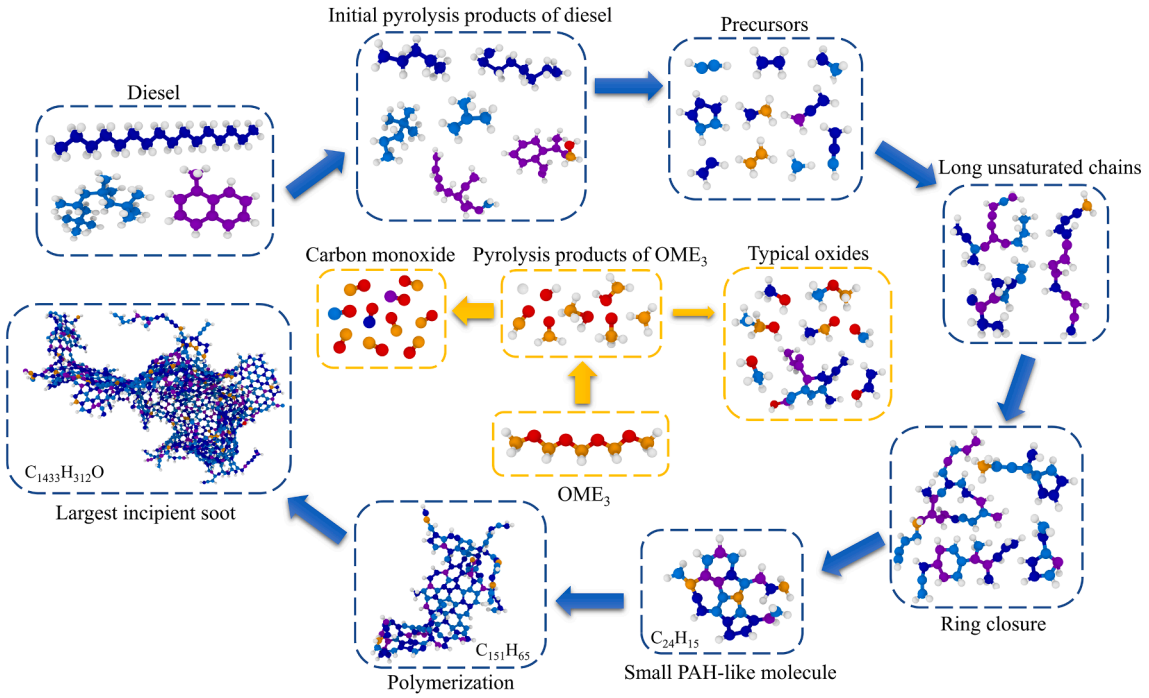

Fig. 13. Reaction pathways of soot inception of diesel-OME_3 pyrolysis and how OME_3 affects the process.

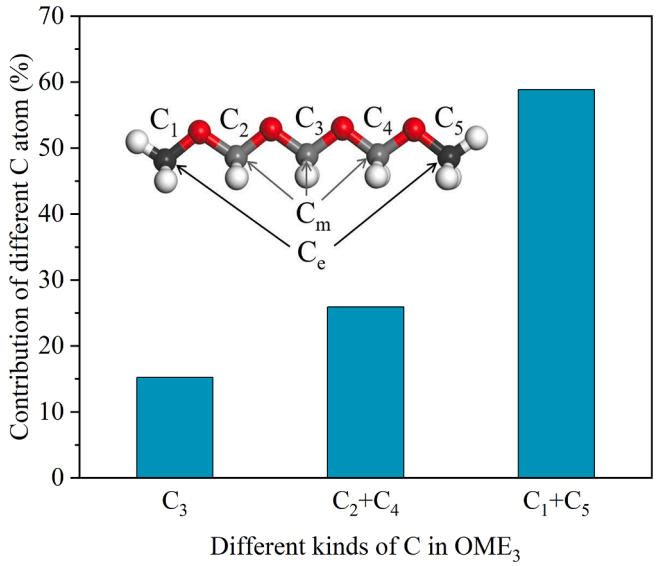

Fig. 14. Contributions of different carbon atoms in OME_3 to incipient soot.

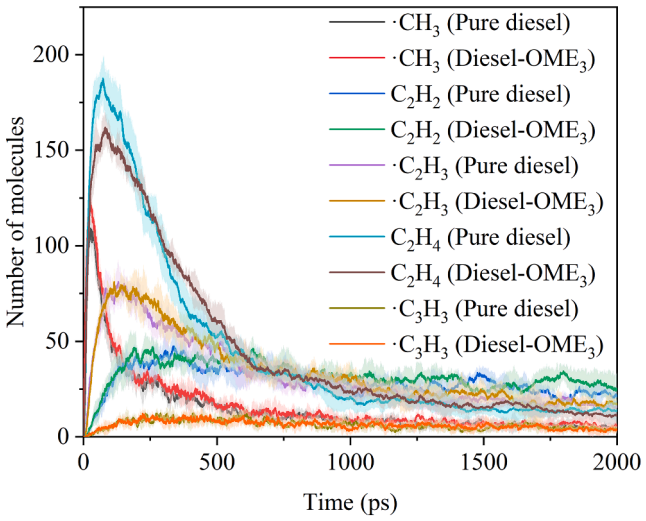

Fig. 15. Time evolutions of typical C_1-C_3 intermediates.

diesel. The •CH_3 molecules produced by OME_3 would connect with these species to form more C_2-C_3 species such as •C_2H_6, C_3H_6,•C_3H_7, and C_4H_7, then these C_2-C_4 species would experience dehydrogenation and β-scission reactions to reproduce C_2H_4. This could also explain why the number of molecules of the main soot precursors C_2H_2, •C_2H_3 and •C_3H_3 do not differ much between pure diesel and diesel-OME_3 blend systems. Although the presence of OME_3 diluted the diesel content, there was no significant reduction in the number of soot precursors due to the presence of •CH_3 produced by OME_3. It needs to be noted that the inclusion of OME_3 would alter the combustion temperature in reality but not in the MD simulations, which is one of the limitations of this work. In general, it is worth noting that the real experimental conditions are quite different from those used in the MD simulations, which were set to speed up the chemical reactions. Although the simulated MD conditions are believed not to significantly affect the reaction pathways, other kinetic parameters such as the reaction rates will be quantitatively affacted.

3.3. Effect of the chain length of OME_X and the content of OME_3 on soot formation in diesel-OMEx systems

Fig. 16 displays the frequency of the addition reactions of •OH radicals with C_1, C_2, and C_3 hydrocarbon species in the blends of diesel with different OME_X (x = 1,3,5). To avoid possible distortion, only reaction occurrences more than once are shown in Fig. 16. It can be seen from the results that •OH radicals mainly react with •CH_3 radicals in every system. As the length of the OME_X chain increases, the oxidative effect of hydroxyl groups on gaseous soot precursors in the system is somewhat enhanced. Also, it is interesting to notice that this effect is nonlinear as OME_X chain length increases. The total number of hydroxyl addition

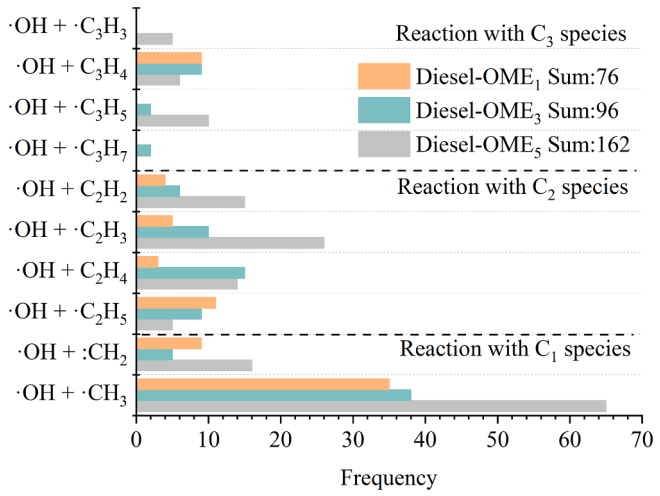

Fig. 16. Frequency of the addition reactions of •OH radicals with C_1, C_2, and C_3 species in diesel-OME_x (x = 1,3,5) systems.

processes increases by 20 from OME_1 to OME_3, but by 66 from OME_3 to OME_5.

Fig. 17 displays the time evolution of the sum of the carbon number of molecules with carbon numbers greater than 40, representing the total carbon number of incipient soot. Fig. 17a shows that when diesel was blended with the same molar fractions of OME_X with different chain lengths, there was no significant reduction in soot inception during the 2 ns simulation period. This simulation result is consistent with the experimental results of Schmitz et al. [61], where they measured the number and size of the soot particles in all OME_{2-4} -blended flames and found that chain length has a minor influence on soot suppression. This is because chain length increase would not increase the effective soot suppression species CH_3O• but CH_2O only. As discussed previously, the follow-up reactions of CH_3O• radicals would produce •OH, which is a powerful soot suppression radical, while the CH_2O molecules would mainly experience the reaction $CH_2O \rightarrow$ •CHO $\rightarrow$ CO to be converted to carbon monoxide and hardly participate in oxidizing soot precursors [53]. Trajectory analysis indicates that a small fraction of CH_2O molecules will form CH_3OH molecules via the reactions CH_2O + •H $\rightarrow$ •CH_2OH and •CH_2OH + •H $\rightarrow$ CH_3OH. Subsequently, some CH_3OH molecules will release •OH radicals, which explains why the oxidative effect is enhanced as the chain length of OME_X increases as shown in Fig. 16.

Fig. 17b shows the time evolution of carbon number above 40 when OME_3 was blended with diesel at 0%, 5%, and 20%. An increase in the proportion of OME_3 from 0% to 20% shows a decreasing trend in incipient soot production. An increase in OME_3 content means a decrease in the diesel fuel content of the system, as the total carbon number is the same in different systems. The presence of carbon in OME_3 dilutes the amount of soot-forming carbon as the total amount of carbon remains unchanged. From 500 to 600 ps, when OME_3 was blended with diesel at 5%, there was no significant reduction in the production of incipient soot, despite some reactive oxygen-containing products and CO are generated during this time. Also, from Table 2, the percentage of carbon atoms in diesel converted to incipient soot even increased slightly in diesel with a 5% OME_3 added system, compared to a pure diesel system. Tan et al. [29] found that when OME_3 was blended with ethylene at 5%, the average soot particle size increased because the •CH_3 produced by OME_3 would react with C_2 species to produce C_3 species, thus activating the $C_3 + C_3$ pathways to form benzene. In this study, the pyrolysis of diesel would produce lots of C_1 and C_2 species, and the pathways of $C_1 + C_1 \rightarrow C_2$ and $C_1 + C_2 \rightarrow C_3$ are both enhanced due to the presence of •CH_3 produced by OME_3. Because only a small amount of OME_3 (5%) was added into diesel, the capabilities of oxygen in OME_3 to trap carbon atoms and the oxidation of soot precursors by oxidation radicals are weaker than the capability of •CH_3 to promote the production of C_2 and C_3 species.

4. Conclusions

In this study, the pyrolysis pathways of OME_3 and the role of OME_3 in the pyrolysis of diesel to form soot have been analysed using ReaxFF-based MD simulations. The MD results revealed the chemical mechanisms involved at the atomic scale. The initial cleavage reactions of OME_3 begin with breaking different C-O bonds and mainly end up with three species: CH_2O, CH_3O•, and •CH_3, of which CH_2O molecule is the predominant product. The CH_3O• and •CH_3 radicals are produced by breaking the C-O bonds at the end edge of OME_3, whereas the CH_2O is produced by breaking the C-O bond in the middle part of OME_3

Table 2
Percentage of carbon atoms in diesel converted to incipient soot.

Pure Diesel	Diesel-5 % OME_3	Diesel-10 %OME_3	Diesel-20 %OME_3	Diesel-40 %OME_3	Diesel-50 %OME_3
80.07 ± 1.72	80.71 ± 1.09	78.05 ± 1.59	76.84 ± 0.68	70.79 ± 1.68	65.69 ± 0.52

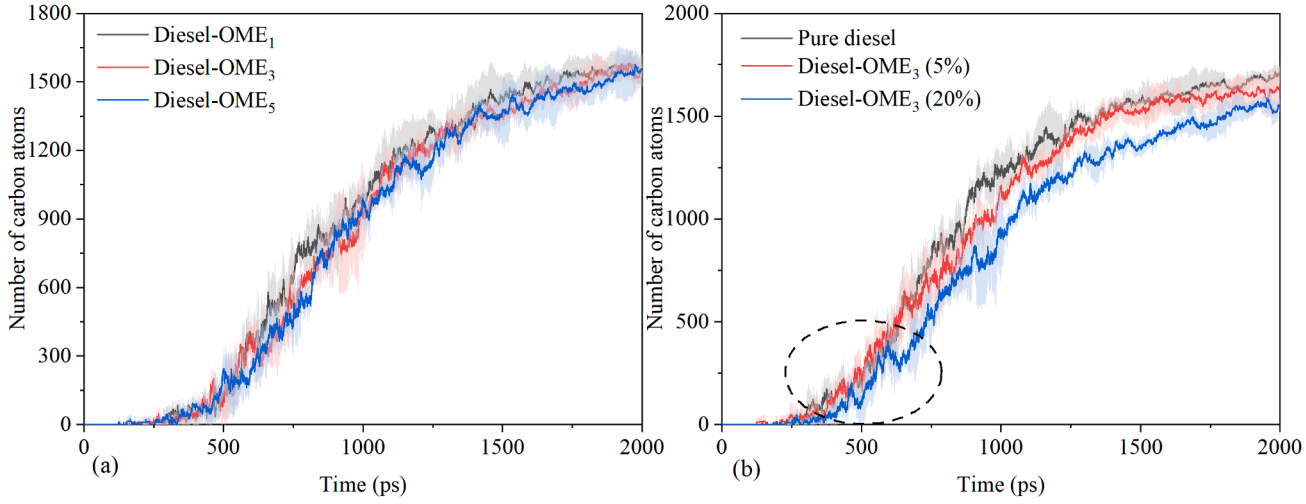

Fig. 17. Time evolution of the sum of the carbon number of molecules with carbon numbers greater than 40: (a) diesel with a different chain length of OME_X added; (b) diesel with different content of OME_3 added.

molecules. The CH_2O is mainly consumed through dehydrogenation to form •CHO, then •CHO would quickly form carbon monoxide through further dehydrogenation. The carbon monoxide would be continuously produced during the whole soot formation process. These carbon atoms would not participate in the production of soot, thus reducing soot formation. The CH_2O and •CHO are less likely to react with other species. The follow-up reactions of CH_3O• would produce oxidizing species such as •OH to oxidize soot precursors. However, this effect is not very significant in the absence of oxygen. The •CH_3 would participate in the formation of soot precursors. As the pyrolysis of diesel would produce lots of C_1 to C_2 unsaturated hydrocarbons, the additional production of •CH_3 from OME_3 pyrolysis could react with these unsaturated C_1-C_2 species, which may lead to increased levels of the main soot precursors such as C_2H_2, •C_2H_3, and •C_3H_3.

A ReaxFF-based panoramic soot inception mechanism of diesel is established in this study. An atomic labeling method was applied to visually illustrate the role of carbon atoms from different components of fuels in the formation of incipient soot. The oxidative effect of adding OME_X on soot formation of diesel has also been investigated. The oxidizing species (mainly •OH, together with CH_3O•, •CHO, and •CH_2OH) produced by OME_3 would react with C_1-C_3 hydrocarbon molecules to form stable oxides.

The effect of chain length of OME_X on diesel soot inhibition was analysed. Increasing the chain length of OME_X could enhance the oxidative effect, while this effect is not significant, as increasing the chain length would mainly increase the amount of CH_2O produced. The CH_2O would rarely participate in oxidizing soot precursors. However, the higher the content of OME_X in the mixture, the fewer carbon atoms are involved in forming soot precursors, as oxygen atoms will mainly fix the carbon in the middle of OME_3 molecules to form carbon monoxide. It is worth noting that if a small amount of OME_X is added to the diesel fuel, the •CH_3 produced by OME_3 may promote the formation of soot.

This study demonstrates the feasibility of ReaxFF-based MD simulations with CHO_{2016} parameters in studying the mechanism of soot inhibition by oxygenated additives. The effect of OME_3 on soot inhibition in a combustion environment can be further investigated, as the presence of oxygen might promote the production of more oxidizing groups, with a more pronounced effect on soot inhibition.

CRediT authorship contribution statement

Zhihao Xing: Conceptualization, Methodology, Software, Writing – original draft. **Mengwei Yu:** Conceptualization, Methodology, Software. **Cheng Chen:** Conceptualization, Methodology, Software. **Xi Jiang:** Conceptualization, Methodology, Supervision, Writing – review & editing.

Declaration of Competing Interest

The authors declare that they have no known competing financial interests or personal relationships that could have appeared to influence the work reported in this paper.

Data availability

Data will be made available on request.

Acknowledgements

Supercomputing time on ARCHER is provided by the "UK Consortium on Mesoscale Engineering Sciences (UKCOMES)" under the UK Engineering and Physical Sciences Research Council Grant No. EP/R029598/1. This work made use of computational support by CoSeC, the Computational Science Centre for Research Communities, through UKCOMES.

References

[1] Adachi K, Buseck PR. Internally mixed soot, sulfates, and organic matter in aerosol particles from Mexico City. Atmos Chem Phys 2008;8:6469–81. https://doi.org/10.5194/acp-8-6469-2008.
[2] Tree DR, Svensson KI. Soot processes in compression ignition engines. Prog Energy Combust Sci 2007;33:272–309. https://doi.org/10.1016/j.pecs.2006.03.002.
[3] Xu L, Wang Y, Liu D. Effects of oxygenated biofuel additives on soot formation: A comprehensive review of laboratory-scale studies. Fuel 2022;313:122635. https://doi.org/10.1016/j.fuel.2021.122635.
[4] Bond TC, Doherty SJ, Fahey DW, Forster PM, Berntsen T, DeAngelo BJ, et al. Bounding the role of black carbon in the climate system: A scientific assessment: BLACK CARBON IN THE CLIMATE SYSTEM. J Geophys Res Atmos 2013;118(11):5380–552.
[5] Frank B, Schlögl R, Su DS. Diesel Soot Toxification. Environ Sci Technol 2013;47:3026–7. https://doi.org/10.1021/es4003873.
[6] Curran HJ, Fisher EM, Glaude P-A, Marinov NM, Pitz WJ, Westbrook CK, et al. Detailed Chemical Kinetic Modeling of Diesel Combustion with Oxygenated Fuels, 2001, pp. 2001-01–0653. https://doi.org/10.4271/2001-01-0653.
[7] Frenklach M. Reaction mechanism of soot formation in flames. Phys Chem Chem Phys 2002;4:2028–37. https://doi.org/10.1039/b110045a.
[8] Erdiwansyah, Mamat R, Sani MSM, Sudhakar K, Kadarohman A, Sardjono RE. An overview of Higher alcohol and biodiesel as alternative fuels in engines. Energy Rep 2019;5:467–79.
[9] Liu H, Wang Z, Wang J, He X. Improvement of emission characteristics and thermal efficiency in diesel engines by fueling gasoline/diesel/PODEn blends. Energy 2016;97:105–12. https://doi.org/10.1016/j.energy.2015.12.110.
[10] Muthuraman VS, Patel A, Shreya V, Vaidyanathan A, Reshwanth KNGL, Karthick C, et al. Progress on compatibility issues of alcohols on automotive materials: Kinetics, challenges and future prospects- a comprehensive review. Process Saf Environ Prot 2022;162:463–93.
[11] Rodríguez-Vallejo DF, Valente A, Guillén-Gosálbez G, Chachuat B. Economic and life-cycle assessment of OME $_{3-5}$ as transport fuel: a comparison of production pathways. Sustainable Energy Fuels 2021;5:2504–16. https://doi.org/10.1039/D1SE00335F.
[12] Liu J, Wang L, Wang P, Sun P, Liu H, Meng Z, et al. An overview of polyoxymethylene dimethyl ethers as alternative fuel for compression ignition engines. Fuel 2022;318:123582. https://doi.org/10.1016/j.fuel.2022.123582.
[13] Chen H, Wang H, Chen Z, Zhao H, Geng L, Gao N, et al. Research progress on the spray, combustion and emission of polyoxymethylene dimethyl ethers as a diesel blend fuel: A review. Fuel 2022;324:124731. https://doi.org/10.1016/j.fuel.2022.124731.
[14] Awad OI, Ma X, Kamil M, Ali OM, Ma Y, Shuai S. Overview of polyoxymethylene dimethyl ether additive as an eco-friendly fuel for an internal combustion engine: Current application and environmental impacts. Sci Total Environ 2020;715:136849. https://doi.org/10.1016/j.scitotenv.2020.136849.
[15] Lumpp B, Rothe D, Pastötter C, Lämmermann R, Jacob E. Oxymethylene ethers as diesel fuel additives of the future. MTZ Worldw 2011;72:34–8. https://doi.org/10.1365/s38313-011-0027-z.
[16] García A, Gil A, Monsalve-Serrano J, Lago SR. OMEx-diesel blends as high reactivity fuel for ultra-low NOx and soot emissions in the dual-mode dual-fuel combustion strategy. Fuel 2020;275:117898. https://doi.org/10.1016/j.fuel.2020.117898.
[17] Huang H, Liu Q, Teng W, Wang Q. The Potentials for Improving Combustion Performance and Emissions in Diesel Engines by Fueling n-butanol/diesel/PODE 3–4 Blends. Energy Proc 2017;105:914–20. https://doi.org/10.1016/j.egypro.2017.03.415.
[18] Omari A, Heuser B, Pischinger S, Rüdinger C. Potential of long-chain oxymethylene ether and oxymethylene ether-diesel blends for ultra-low emission engines. Appl Energy 2019;239:1242–9. https://doi.org/10.1016/j.apenergy.2019.02.035.
[19] Li R, Herreros JM, Tsolakis A, Yang W. Chemical kinetic study on ignition and flame characteristic of polyoxymethylene dimethyl ether 3 (PODE3). Fuel 2020;279:118423. https://doi.org/10.1016/j.fuel.2020.118423.
[20] Burger J, Siegert M, Ströfer E, Hasse H. Poly(oxymethylene) dimethyl ethers as components of tailored diesel fuel: Properties, synthesis and purification concepts. Fuel 2010;89:3315–9. https://doi.org/10.1016/j.fuel.2010.05.014.
[21] Liu H, Wang Z, Wang J, He X, Zheng Y, Tang Q, et al. Performance, combustion and emission characteristics of a diesel engine fueled with polyoxymethylene dimethyl ethers (PODE3-4)/ diesel blends. Energy 2015;88:793–800.
[22] Liu J, Wang Hu, Li Y, Zheng Z, Xue Z, Shang H, et al. Effects of diesel/PODE (polyoxymethylene dimethyl ethers) blends on combustion and emission characteristics in a heavy duty diesel engine. Fuel 2016;177:206–16.
[23] Popp T, Lechner R, Becker M, Hebauer M, O'Connell N, Brautsch M. Potentials of OME/diesel blends for stationary power production – Improving emission characteristics of a diesel CHP unit. Appl Therm Eng 2019;153:483–92. https://doi.org/10.1016/j.applthermaleng.2019.03.015.
[24] Lin Q, Tay KL, Yu W, Yang W, Wang Z. Effects of polyoxymethylene dimethyl ether 3 (PODE3) addition and injection pressure on combustion performance and particle size distributions in a diesel engine. Fuel 2021;283:119347. https://doi.org/10.1016/j.fuel.2020.119347.
[25] Liu H, Wang Z, Zhang J, Wang J, Shuai S. Study on combustion and emission characteristics of Polyoxymethylene Dimethyl Ethers/diesel blends in light-duty and heavy-duty diesel engines. Appl Energy 2017;185:1393–402. https://doi.org/10.1016/j.apenergy.2015.10.183.

[26] Lautenschütz L, Oestreich D, Seidenspinner P, Arnold U, Dinjus E, Sauer J. Physico-chemical properties and fuel characteristics of oxymethylene dialkyl ethers. Fuel 2016;173:129–37. https://doi.org/10.1016/j.fuel.2016.01.060.
[27] Yu M, Chen C, Jiang X. Understanding the miscibility of polyoxymethylene dimethyl ethers (OMEn) and diesel blend using molecular dynamics simulation. Fuel 2022;323:124348. https://doi.org/10.1016/j.fuel.2022.124348.
[28] Omari A, Heuser B, Pischinger S. Potential of oxymethylenether-diesel blends for ultra-low emission engines. Fuel 2017;209:232–7. https://doi.org/10.1016/j.fuel.2017.07.107.
[29] Tan YR, Salamanca M, Pascazio L, Akroyd J, Kraft M. The effect of poly (oxymethylene) dimethyl ethers (PODE3) on soot formation in ethylene/PODE3 laminar coflow diffusion flames. Fuel 2021;283:118769. https://doi.org/10.1016/j.fuel.2020.118769.
[30] Lin Q, Tay KL, Yu W, Zong Y, Yang W, Rivellini L-H, et al. Polyoxymethylene dimethyl ether 3 (PODE3) as an alternative fuel to reduce aerosol pollution. J Clean Prod 2021;285:124857. https://doi.org/10.1016/j.jclepro.2020.124857.
[31] Ferraro F, Russo C, Schmitz R, Hasse C, Sirignano M. Experimental and numerical study on the effect of oxymethylene ether-3 (OME3) on soot particle formation. Fuel 2021;286:119353. https://doi.org/10.1016/j.fuel.2020.119353.
[32] Liu Y, Cheng X, Ya Y, Wang B, Zhang P, Zhang K, et al. Impact of PODE3 on soot oxidation reactivity at different stages in n-heptane/toluene diffusion flames. Fuel 2023;331:125672. https://doi.org/10.1016/j.fuel.2022.125672.
[33] Pastor JV, García A, Micó C, Lewiski F. Simultaneous high-speed spectroscopy and 2-color pyrometry analysis in an optical compression ignition engine fueled with OMEX-diesel blends. Combust Flame 2021;230:111437. https://doi.org/10.1016/j.combustflame.2021.111437.
[34] García-Oliver JM, Novella R, Micó C, Bin-Khalid U. A numerical investigation of the performance of oxymethylene ethers blended with fossil diesel to reduce soot emissions in compression ignition engines. Fuel 2022;324:124768. https://doi.org/10.1016/j.fuel.2022.124768.
[35] Cai P, Zhang C, Jing Z, Chen Z. Development and validation of a reduced polyoxymethylene dimethyl ether 3 – Biodiesel reaction mechanism for engine application. Fuel 2021;291:120144. https://doi.org/10.1016/j.fuel.2021.120144.
[36] Mao Q, van Duin ACT, Luo KH. Formation of incipient soot particles from polycyclic aromatic hydrocarbons: A ReaxFF molecular dynamics study. Carbon 2017;121:380–8. https://doi.org/10.1016/j.carbon.2017.06.009.
[37] Kwon H, Etz BD, Montgomery MJ, Messerly R, Shabnam S, Vyas S, et al. Reactive Molecular Dynamics Simulations and Quantum Chemistry Calculations To Investigate Soot-Relevant Reaction Pathways for Hexylamine Isomers. J Phys Chem A 2020;124(21):4290–304.
[38] Wang Y, Gu M, Zhu Y, Cao L, Wu J, Lin Y, et al. Analysis of soot formation of CH4 and C2H4 with H2 addition via ReaxFF molecular dynamics and pyrolysis–gas chromatography/mass spectrometry. J Energy Inst 2022;100:177–88.
[39] Chen C, Jiang X. Molecular dynamics simulation of soot formation during diesel combustion with oxygenated fuel addition. Phys Chem Chem Phys 2020;22:20829–36. https://doi.org/10.1039/D0CP01917H.
[40] van Duin ACT, Dasgupta S, Lorant F, Goddard WA. ReaxFF: A Reactive Force Field for Hydrocarbons. J Phys Chem A 2001;105:9396–409. https://doi.org/10.1021/jp004368u.
[41] Chenoweth K, van Duin ACT, Goddard WA. ReaxFF Reactive Force Field for Molecular Dynamics Simulations of Hydrocarbon Oxidation. J Phys Chem A 2008;112:1040–53. https://doi.org/10.1021/jp709896w.
[42] Ashraf C, van Duin ACT. Extension of the ReaxFF Combustion Force Field toward Syngas Combustion and Initial Oxidation Kinetics. J Phys Chem A 2017;121:1051–68. https://doi.org/10.1021/acs.jpca.6b12429.
[43] Pitz WJ, Mueller CJ. Recent progress in the development of diesel surrogate fuels. Prog Energy Combust Sci 2011;37:330–50. https://doi.org/10.1016/j.pecs.2010.06.004.
[44] Qian Y, Yu L, Li Z, Zhang Y, Xu L, Zhou Q, et al. A new methodology for diesel surrogate fuel formulation: Bridging fuel fundamental properties and real engine combustion characteristics. Energy 2018;148:424–47.
[45] Plimpton S. Fast Parallel Algorithms for Short-Range Molecular Dynamics. J Comput Phys 1995;117:1–19. https://doi.org/10.1006/jcph.1995.1039.
[46] Mayo SL, Olafson BD, Goddard WA. DREIDING: a generic force field for molecular simulations. J Phys Chem 1990;94:8897–909. https://doi.org/10.1021/j100389a010.
[47] Zhao J, Lin Y, Huang K, Gu M, Lu K, Chen P, et al. Study on soot evolution under different hydrogen addition conditions at high temperature by ReaxFF molecular dynamics. Fuel 2020;262:116677. https://doi.org/10.1016/j.fuel.2019.116677.
[48] Wang L, Sun W, Yang Q. Exploration of the Influences of the PODE $_3$ Additive on the Initial Pyrolysis of Diesel by ReaxFF Molecular Dynamics Simulations. Energy Fuels 2021;35:9825–35. https://doi.org/10.1021/acs.energyfuels.1c00074.
[49] Cheng X-M, Wang Q-D, Li J-Q, Wang J-B, Li X-Y. ReaxFF Molecular Dynamics Simulations of Oxidation of Toluene at High Temperatures. J Phys Chem A 2012;116:9811–8. https://doi.org/10.1021/jp304040q.
[50] Stukowski A. Visualization and analysis of atomistic simulation data with OVITO-the Open Visualizati. Model Simul Mater Sci Eng 2010:8. https://doi.org/10.1088/0965-0393/18/1/015012.
[51] Zeng J, Cao L, Chin C-H, Ren H, Zhang JZH, Zhu T. ReacNetGenerator: an automatic reaction network generator for reactive molecular dynamics simulations. Phys Chem Chem Phys 2020;22:683–91. https://doi.org/10.1039/C9CP05091D.
[52] Sun W, Wang G, Li S, Zhang R, Yang B, Yang J, et al. Speciation and the laminar burning velocities of poly(oxymethylene) dimethyl ether 3 (POMDME3) flames: An experimental and modeling study. Proc Combust Inst 2017;36(1):1269–78.
[53] Tan YR, Botero ML, Sheng Y, Dreyer JAH, Xu R, Yang W, et al. Sooting characteristics of polyoxymethylene dimethyl ether blends with diesel in a diffusion flame. Fuel 2018;224:499–506.
[54] Huang H, Liu Q, Teng W, Pan M, Liu C, Wang Q. Improvement of combustion performance and emissions in diesel engines by fueling n-butanol/diesel/PODE3–4 mixtures. Appl Energy 2018;227:38–48. https://doi.org/10.1016/j.apenergy.2017.09.088.
[55] Westbrook CK, Dryer FL. Chemical kinetic modeling of hydrocarbon combustion. Prog Energy Combust Sci 1984;10:1–57. https://doi.org/10.1016/0360-1285(84)90118-7.
[56] Liu L, Chen S, Xu H, Zhu Q, Ren H. Effect of alkyl substituent for cyclohexane on pyrolysis towards sooting tendency from theoretical principle. J Anal Appl Pyrol 2022;161:105386. https://doi.org/10.1016/j.jaap.2021.105386.
[57] Zheng Mo, Li X, Liu J, Wang Ze, Gong X, Guo Li, et al. Pyrolysis of Liulin Coal Simulated by GPU-Based ReaxFF MD with Cheminformatics Analysis. Energy Fuels 2014;28(1):522–34.
[58] Han S, Li X, Zheng M, Guo L. Initial reactivity differences between a 3-component surrogate model and a 24-component model for RP-1 fuel pyrolysis evaluated by ReaxFF MD. Fuel 2018;222:753–65. https://doi.org/10.1016/j.fuel.2018.02.112.
[59] Johansson KO, Head-Gordon MP, Schrader PE, Wilson KR, Michelsen HA. Resonance-stabilized hydrocarbon-radical chain reactions may explain soot inception and growth. Science 2018;361:997–1000. https://doi.org/10.1126/science.aat3417.
[60] Han S, Li X, Nie F, Zheng M, Liu X, Guo L. Revealing the Initial Chemistry of Soot Nanoparticle Formation by ReaxFF Molecular Dynamics Simulations. Energy Fuels 2017;31:8434–44. https://doi.org/10.1021/acs.energyfuels.7b01194.
[61] Schmitz R, Russo C, Ferraro F, Apicella B, Hasse C, Sirignano M. Effect of oxymethylene ether-2-3-4 (OME2-4) on soot particle formation and chemical features. Fuel 2022;324:124617. https://doi.org/10.1016/j.fuel.2022.124617.